Composite Structures 295 (2022) 115864

Contents lists available at ScienceDirect

Composite Structures

journal homepage: www.elsevier.com/locate/compstruct

Suppression of the sutural interface on vibration behaviors of sandwich beam with shear stiffening gel

Xiwen Fan, Yu Wang *, Sheng Wang, Xinglong Gong *

CAS Key laboratory of Mechanical Behavior and Design of Materials, Department of Modern Mechanics, University of Science and Technology of China (USTC), Hefei 230027, China

ARTICLE INFO

Keywords:
Sutural interface
Sandwich structure
Shear stiffening gel (SSG)
Vibration

ABSTRACT

Sutural composites have been widely adopted as structural components in various engineering applications. In this work, a series of sutural sandwich beam were prepared by integrating the magneto-rheological shear stiffening gel (SSG) and 3D-printed face sheet material. The structural stiffness of beam samples with different sutural interface was tested. It could be found that the sutural interface geometry showed significant influence on the structural stiffness. Due to the specific viscoelastic property of SSG material, the damping ratio of the beam could be improved with the sutural interface. Meanwhile, benefitted from the rate-dependent stiffening and magneto-rheological properties of the SSG core, the sandwich beams exhibited passive and active vibrations suppression capacities. A theory model about the transmission of the beam with SSG core under external vibration excitation was carried out to explain the experimental results. This work proved that the sutural interface could be adopted as a promising strategy to improve the structural stiffness and vibration control capability of the sandwich beam, which was every important in the application of many industry fields.

1. Introduction

Biological materials have attracted much attention because they provide excellent solutions to balance the stiffness, strength and toughness via sophisticated microstructures [1–4]. Natural composites can evolve into optimal architectures to achieve different biological functions such as loading transmission [5], energy absorption [6] and penetration resistance [7]. Among these diverse geometries, sutural interfaces have been widely studied because of its designable mechanical principles [8–11]. Generally, sutural composites are composed of two stiff skin face sheets and soft core materials [12]. The mechanical properties significantly depend on the structural materials and interface geometry design. Tounsi el al. [13–15] explored the influence of material parameters and panel geometry configurations on the characteristics of vibration and stress propagation in the sandwich structure. Besides, ambient conditions also affected its mechanical performance. M. Al-Zahrani el al. [16,17] investigated the vibration and wave propagation of the functionally graded sandwich plate in a hygro-thermal environment, revealing their reliance on moisture and temperature. Thus, by carefully designing the interface geometry and applying the external field, the mechanical properties could be artificially improved.

Compared to conventional staggered composites, the inclined interfaces of sutural composites changed the transmission mechanisms of stress [18,19]. Shear stress played same important role as the normal stress do. By designing the parameters of sutural interfaces, Li et al. [11,18] adopted a continuous model to analysis the equivalent stiffness of different sutural interfaces with the sutural shape in triangular, trapezoidal, rectangular, and anti-trapezoidal waveforms, etc. Furthermore, Yu et al. [20] developed an analytical model to analyze the effect of visco-elastic properties of core material on the dynamic mechanical of sutural composites. Jia et al. [21] compared the toughness of different biomimetic architected materials under impact loading case. The above results show that appropriate structural design and material selection for the sutural interface could effectively improve the mechanical properties of sutural composites.

Natural sandwich composites are always exposed to various environmental stimulus. Large numbers of researches have pointed out that appropriate stiffness ratio of stiff skin and soft core can effectively improve the dynamic behaviors of sandwich composites[22–24]. To obtain higher structural stiffness or higher damping factors, various smart materials, such as artificial suspensions and gel composites, were used as core materials to achieve higher mechanical performance under

* Corresponding authors.
E-mail addresses: wyu@ustc.edu.cn (Y. Wang), gongxl@ustc.edu.cn (X. Gong).

https://doi.org/10.1016/j.compstruct.2022.115864
Received 7 November 2021; Received in revised form 28 April 2022; Accepted 1 June 2022
Available online 6 June 2022

different external excitation in engineering application. Here, the shear stiffening gel (SSG), a kind of hybrid polyboronsiloxane with typical rate-dependent behaviors[25,26], was adopted as the core material. The rate-dependent properties of SSG would permit the sandwich composites to withstand high dynamic loading and dissipate the kinetic energy in short time [27,28].

In this work, sutural sandwich beam structures were designed. The skin face-sheets were fabricated by 3D printing method. SSG with carbonyl iron particles was adopted as the core material. Rheological tests were conducted to characterize the viscoelastic properties of SSG. Three-point bending tests were performed to investigate the flexural stiffness and rate-dependent behaviors of sutural composites. To investigate the vibration behaviors of sutural composites, the sutural composite structures were excited in harmonic modes and its dynamic characteristics were monitored. And in the end, the effects of the magnetic field on the dynamics behaviors were explored for the future application in active control device. Our studies pointed out that the appropriate design of sutural interface could effectively improve the suppression capacity of structural composites on vibration.

2. Experiments and characterization

2.1. Materials and preparation

The raw materials of SSG included as follows: boric acid, caprylic acid (Sinopharm Chemical Reagent Co.Ltd, Shanghai, China), hydroxyl silicone oil (500 mm^2/s, AR degree, Jining Huakai Resin Co.Ltd), carbonyl iron particles (CIPs, type CN. BASF, Germany). The boric acid and silicone oil were mixed at the mass ratio of 1:15 and heated at 180 °C for 2 h. 15 μl caprylic acid was poured into every 100 g suspensions (Fig. 1a). After another hour of heating, CIPs were added into the paste with the mass ratio of 50% (Fig. 1b). Then, the magneto-rheological SSG was obtained. Polydimethylsiloxane (PDMS) was adopted as control group to ensure the influence of SSG.

The skin facesheets were printed using polylactic acid (PLA) by a 3D printer (Creator 3, Flashforge Co., China). The sizes of specimens were shown in Fig. 2. The thickness of sutural composites was 20 mm. The length and width were 180 mm and 20 mm, respectively. The height of slant waveform was 9.6 mm. By adjusting the numbers of triangular waves, the vertex angles θ ranged from 30°, 45°, 60° to 180°.

2.2. Characterization

The rheological behaviors of SSG were tested by a commercial rheometer (Physica MCR 302, Anton Paar Co., Austria). Parallel plate was adopted to test the rate-dependent and magnetic dependent behaviors of SSG. Sample specimens were molded into a circle plate with 1 mm in height and 20 mm in diameter. Magnetic field was generated by a programmable power supply (ITECH Electronic Co. Ltd, China).

Three-point bending tests were conducted by a universal testing machine (Fig. 3) (MTS criterion 43, MTS System Co., America). The compressive speeds were controlled at 0.04 mm/s, 0.20 mm/s, and 1.00 mm/s, respectively. The radius of indenter was 8 mm.

The forced vibration experiment was conducted to investigate dynamics characteristics of the sutural composite structure. Two identical beam specimens were fixed in the testing devices as shown in Fig. 4, which were fixed at the middle of the vibration source with plugs. The fixed length was 10 mm and the free length was 170 mm. Three piezoelectric acceleration sensors were fixed at the free end, the middle and the fixed end of the beam specimen to monitor the motion of different points. Furthermore, a parallel magnetic field was generated by a pair of permanent magnets (Fig. 4a). By changing the distance of magnets, the magnetic flux density can range from 0 to 0.3 T. All sensor data were gathered synchronously by a digital acquisition system, including a charge amplifier (Mode YE5853, Jiangsu Sinocera Piezotronics. INC., China) and an oscilloscope (Mode DPO2012B, Tektronix INC., USA).

3. Results and discussion

3.1. Rheological properties of SSG

The rheological properties of SSG were firstly investigated (Fig. 5). The shear amplitude was 0.1% and the environmental temperature was controlled at 25 °C. The rate dependent behaviors of SSG were remarkable. The storage modulus of SSG was 17.86 kPa at the initial 0.628 rad/s. When the shear rate increased to 62.8 rad/s, the storage modulus gradually came into plateau period. It achieved 753.93 kPa at 628 rad/s. The typical rate-dependent behaviors could be also illustrated in loss modulus. The loss modulus obtained peak value, 335.82 kPa, when the shear rate was 9.96 rad/s. Then, it fell down to 24.98 kPa. The rate-dependent behaviors of SSG should be owed to the break and reattachment of the transient "B-O" bonds. When the shear rate was low, it permitted enough time for B-O bonds to break up. The gel matrix showed soft and deformable behaviors. As the shear rate exceeded the relaxation rate of B-O bonds, the motion of gel chains was hindered and large numbers of agglomerations were generated. The gel matrix became stiff.

The enhancement of magnetic field was also remarkable. Soft magnetic particles were induced to agglomerate into clusters in the direction of magnetic field, which provided additional stress to resist deformation. With the increase of magnetic field from 0.1 T to 0.3 T, the storage modulus of SSG increased from 405.82 kPa to 790.58 kPa at 0.628 rad/s. Meanwhile, the loss modulus increased to 276.88 kPa. SSG still held rate-dependent behaviors under different magnetic field. When the

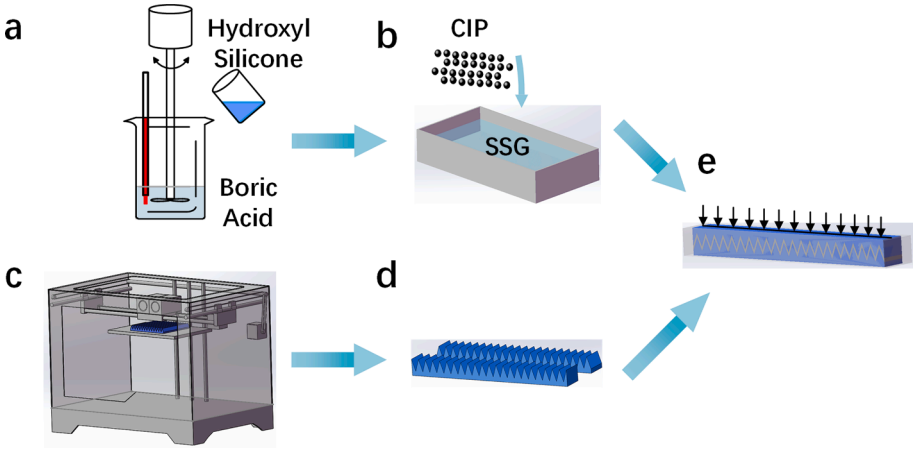

Fig. 1. Fabrication of sutural beam composites.

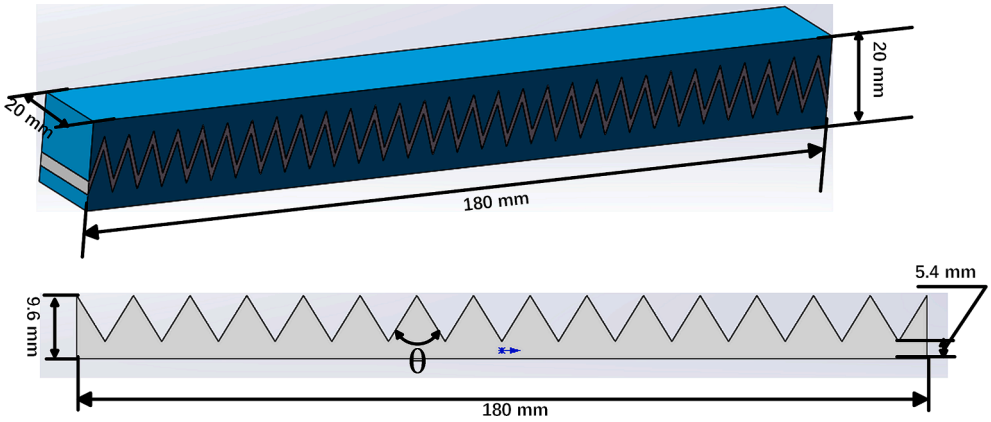

Fig. 2. The dimensions of sutural composites.

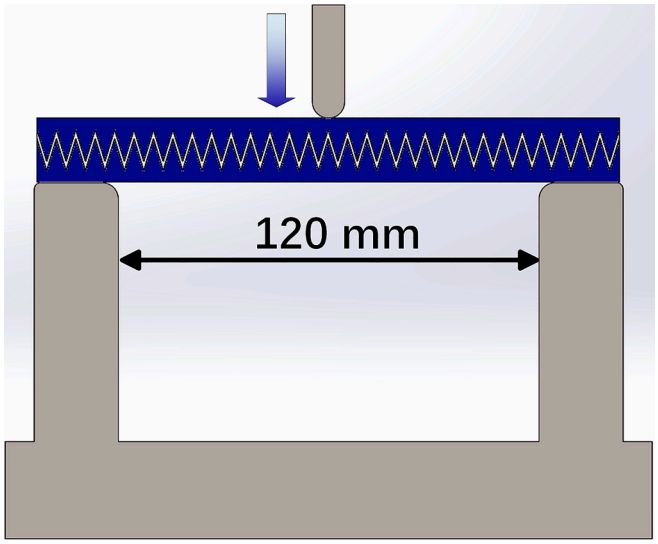

Fig. 3. The three-point bending testing device.

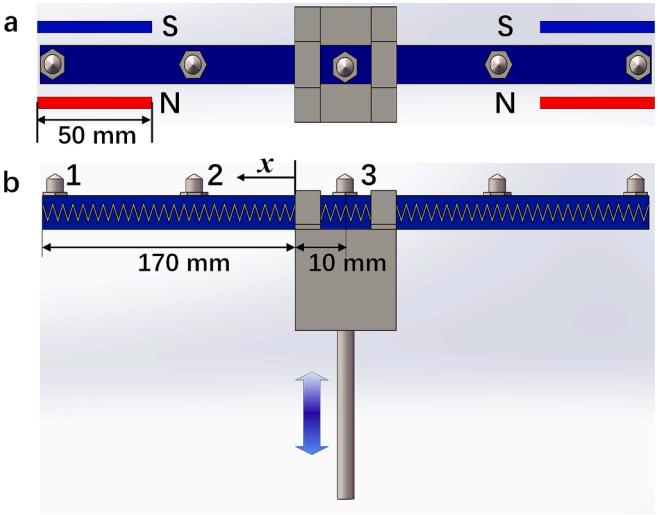

Fig. 4. The schematic forced vibration devices of cantilevered beam. (a) vertical view. (b) front view.

shear rate increased to 628 rad/s, the enhancement amplitude of storage modulus induced by magnetic fields was 255%, 169%, and 124%. This unique behavior provided favorable conditions to achieve the active and passive adjustment of structural stiffness.

3.2. Three-point bending tests

The structural stiffness was tested via three-point bending device. It could be observed that the sutural interfaces heavily influenced the structural stiffness of beam specimens. Sutural angles with 45° and 30° showed remarkable enhancement. 180° sutural beam held nearly linear elastic behaviors when the deformation was smaller than 1.4 mm. Then, the force curve came into a plateau, which illustrated the yield and failure mechanical behaviors in the composite beam. Under the loading speed of 0.04 mm/s, the maximum deformation of 180° sample was 18.92 mm, and the force capacity was 0.31 kN. Meanwhile, the maximum force capacity of 45° and 30° sample was 0.48 kN and 0.52 kN. Compared to 180° sample, the maximum force capacity got an improvement of 55% and 68%. Meanwhile, the structural stiffness showed a growth of 94% and 116%, respectively. Under the large deformation, sutural interface contributed to achieve strain hardening. The slopes of force–displacement came to increase after the 5 mm when the sutural angles were 45° and 30°. However, sutural angles with 60° showed negative influence on the structural stiffness. With the loading rate increased to 0.20 mm/s and 1.00 mm/s, the failure deformation 60° sutural beam was enlarged to 18.83 mm and 19.40 mm.

Compared to 180° sample, sutural composite beam showed more remarkable rate-dependent behaviors under linear scope. With the loading speeds increased from 0.04 mm/s to 1.00 mm/s, the maximum force capacity of 30° sample increased from 0.52 kN to 0.59 kN, yet that of 180° sample held nearly constant. Fig. 6d showed the linear region of different samples. The stiffness of 30° sample was 6.48 times than that of 180° sample. Meanwhile, 60° sample could withstand larger bending deformation. When the deformation was beyond 12 mm, the bending force of 180° sutural beam came to decrease with the increase of deformation. Remarkable strain hardening behaviors could be observed in 60° sutural beam. The tangent slope of force-distance curve of 60° sutural beam increased from 12.28 N/mm to 52.17 N/mm. Proper design of the interfaces could make for achieving high structure stiffness or failure strain.

3.3. Vibration tests with cantilever beam

To investigate the internal material damping behaviors of beam specimen, the functional composites in this work were excited under harmonic vibration to obtain stable response. Here, the motion of cantilever beam was limited in vertical direction. Firstly, theory model was established. The local coordinate axis was established from the fixed

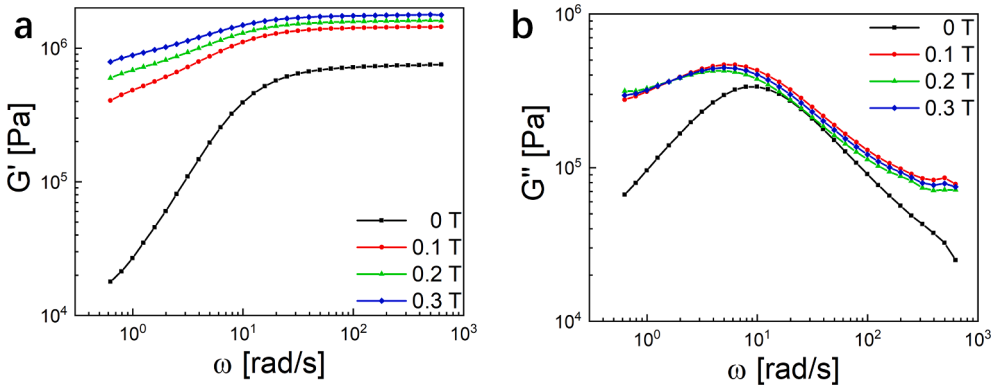

Fig. 5. The rheological properties of SSG. (a) storage modulus, (b) loss modulus.

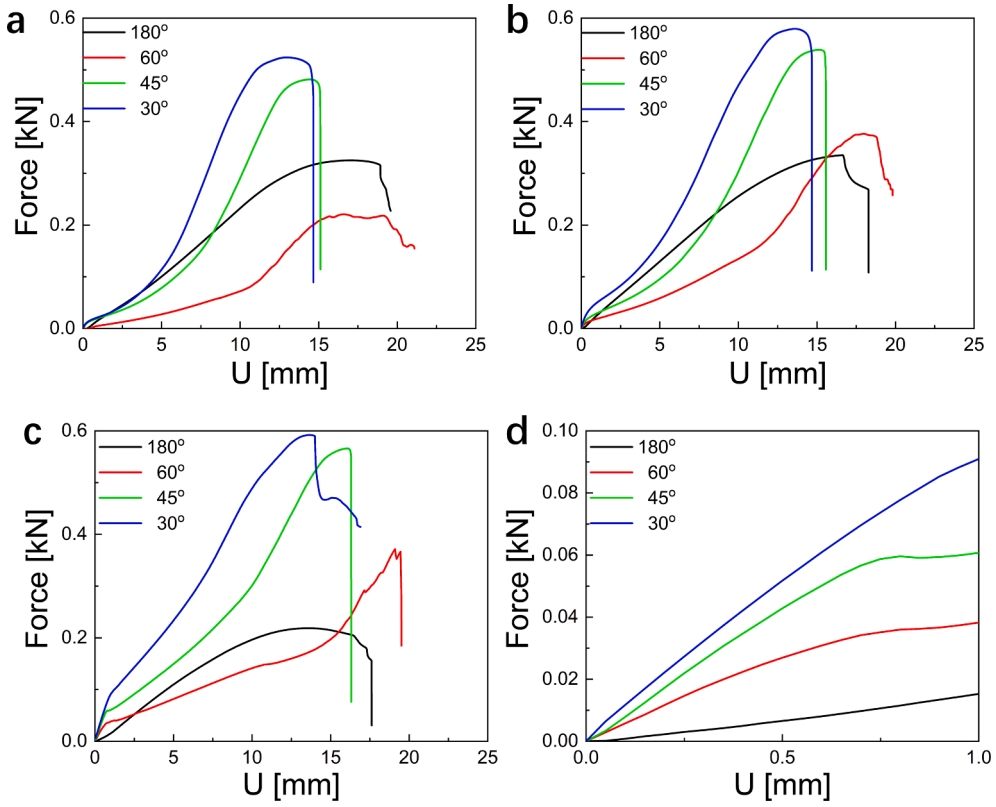

Fig. 6. The force–displacement under different loading speeds. (a) 0.04 mm/s, (b) 0.20 mm/s, (c) 1.00 mm/s. (d) was the linear regions of (c).

end point of cantilever beam (Fig. 4b). The vertical motion of beam was defined as $v(x,t)$. Under harmonic excitation, the control equations of cantilever beam could be expressed as follows:

$$\frac{\partial^2}{\partial x^2}\left[EI\frac{\partial^2 v(x,t)}{\partial x^2}+cI\frac{\partial^3 v(x,t)}{\partial x^2 \partial t}\right]+\rho A\frac{\partial^2 v(x,t)}{\partial t^2}+c\frac{\partial v}{\partial t}=P(x,t) \tag{1}$$

$P(x,t)$ was the equivalent distributed loading due to the external excitation from vibration source. EI was the equivalent flexural stiffness of the whole structure. c was the equivalent viscosity. ρ was the equivalent density and A was the cross sectional area of cantilever beam. The boundary conditions could be obtained:

$$\begin{cases} v(0,t)=\delta sinwt \; v'(0,t)=0 \\ v''(l,t)=0 \; v'''(l,t)=0 \end{cases}$$

The whole vertical displacement of beam could be divided into rigid displacement and deflection:

$$v(x,t)=v_s+v_d \tag{2}$$

Where v_s indicated rigid displacement and v_d indicated the deflection. The v_s was caused by the motion of vibration source and v_d along the cantilever beam was caused by inertial effect. Considering the free end of beam, it could be obtained that:

$$v_s(x,t)=\delta sinwt \tag{3}$$

v_d could be regarded as the deformation led by a linear loading force, $p_d(x,t)$, along the beam. In this way, the external force loading, $p_d(x,t)$ could be regarded as follows:

$$p_d(x,t)=\rho A\frac{x}{l}\delta w^2 sinwt \tag{4}$$

The displacement boundary was transformed into force loading. Then, the control equation and boundary conditions for deflection v_d could be expressed:

$$\begin{cases} \dfrac{\partial^2}{\partial x^2}\left[EI\dfrac{\partial^2 v_d(x,t)}{\partial x^2}+cI\dfrac{\partial^3 v_d(x,t)}{\partial x^2\partial t}\right]+\rho A\dfrac{\partial^2 v_d(x,t)}{\partial t^2}+c\dfrac{\partial v_d}{\partial t}=p_d(x,t) \\ v_d(0,t)=0 v_d{}'(0,t)=0 \\ v_d{}''(l,t)=0 v_d{}'''(l,t)=0 \end{cases} \tag{5}$$

Generally, the solution of v_d could be expressed:

$$v_d = q(t)\varphi(x)$$

Where $q(t)$ was the time term and $\varphi(x)$ was the vibration mode function. Generally, the vibration mode function could be expressed as:

$$\varphi(x) = C_1 sin(\alpha x) + C_2 cos(\alpha x) + C_3 cosh(\alpha x) + C_4 sinh(\alpha x)$$

Based on this boundary conditions of equation (5), the vibration mode function could be expressed as:

$$\varphi(x) = cosh(\alpha x) - cos(\alpha x) + \frac{cos\alpha + cosh\alpha}{sin\alpha + sinh\alpha}[sin(\alpha x) - sinh(\alpha x)] \tag{6}$$

$$\alpha l = 1.8751$$

The natural frequency of cantilever beam was:

$$w_n = (\alpha l)^2\sqrt{\frac{EI}{\rho A l^4}} \tag{7}$$

The generalized mass:

$$M = \frac{\rho A l}{2} \tag{8}$$

And the generalized loading:

$$P(t) = \int_0^l \rho A\frac{x}{l}\delta w^2 sinwt\varphi(x)dx = \frac{\rho A\delta w^2 sinwt}{l}C \tag{9}$$

$$C = 0.0055$$

Equation (5) could be simplified as:

$$\ddot{q}(t) + 2\xi\beta\dot{q}(t) + w^2 q(t) = \frac{P}{M} \tag{10}$$

where the ξ was damping ratio and β was frequency ratio. The solution for equation (10) was:

$$q(t) = \frac{2\rho ACl^2\delta w^2}{(\alpha l)^4 EI}\left(\frac{(1-\beta^2)sinwt - 2\xi\beta coswt}{(1-\beta^2)^2 + (2\xi\beta)^2}\right) \tag{11}$$

Then, the solution for equation (1) could be obtained:

$$v(x,t) = \delta sinwt + \sum\frac{2C_n\delta\beta^2}{l^2}\left(\frac{(1-\beta^2)sinwt - 2\xi\beta coswt}{(1-\beta^2)^2 + (2\xi\beta)^2}\right)\varphi(x) \tag{12}$$

when $x = \frac{l}{2}, x = l$, it could be obtained:

$$\begin{cases} \varphi\left(\dfrac{l}{2}\right) = 0.606 \\ \varphi(l) = 1.510 \end{cases}$$

For every point in the cantilever beam, the motion form could be regarded as forced harmonic vibration, which could be expressed as:

$$v(x,t) = v(x)_0 \sin(wt + \theta)$$

where w was the external excitation rate and θ was the phase difference. In this way, the following equation could be obtained:

$$\overline{v}(0) : \overline{v}\left(\frac{l}{2}\right) : \overline{v}(l) = \overline{\overline{v}}(0) : \overline{\overline{v}}\left(\frac{l}{2}\right) : \overline{\overline{v}}(l) \tag{13}$$

Commonly, the transmission was defined as the ratio of displacement:

$$D_p(x) = \frac{\overline{v(x) - v(0)}}{\overline{v(0)}} = \sum\frac{2\rho ACl^2 w^2}{(\alpha l)^4 EI}\left(\frac{1}{(1-\beta^2)^2 + (2\xi\beta)^2}\right)^{\frac{1}{2}}\varphi(x) \tag{14}$$

Based on equation (11), it could be concluded that the transmission could be calculated by the ratio of acceleration when the external excitation was harmonic form. The damping ratio and natural frequency could be obtained from equation (14).

Fig. 7 showed the motions of the free end point, the middle point and the fixed point of the cantilever beam. The amplitudes of acceleration under different frequencies were obtained by Fourier transform of the raw acceleration signal. The transmission ratio was fitted based on equation (14). Firstly, the influence of SSG was tested under 180° sutural beam compared to PDMS.

Fig. 8 showed the vibration modes of 180° sutural beam with different core materials. Generally, the PDMS was a kind of elastic material with low viscosity. Owing to the high modulus of PDMS, the resonance frequency of beam sample with PDMS was higher than sample with SSG. The low viscosity also led to high transmission of PDMS sutural beam. The transmission at free end point of PDMS sample achieved its peak value, 36.03, when the excitation frequency reaches 80 Hz. At the middle of beam, the transmission was 12.03. The introduction of SSG effectively suppressed the vibration of cantilever beam. The transmission at free end point and middle points were 13.38 and 3.63. Compared to the PDMS beam, it made a reduction of 71% and 70%. When the excitation frequency came to 100 Hz, transmission of PMDS beam was 6.23. The transmission of SSG beam was only 3.05, which showed excellent suppression on the vibration. Based on equation (14), the vibration motion was fitted and results were shown in dash lines. It could be observed that the dash lines could fit the peak values well. The damping ratio of PDMS sutural beam was 2.14%. When it came to SSG sutural beam, the damping ratio was 11.99%. High viscosity of SSG enhanced the attenuation of vibration.

Then, the influence of sutural interface on vibration behaviors was investigated. Fig. 9 illustrated the vibration behaviors of different sutural beam composites. The amplitude of vibration source was 0.1 mm. Excitation frequency ranged from 1 Hz to 150 Hz. 180° sutural beam showed typical visco-elastic beam characterization. Damping transmission achieved its peak value at 62 Hz. The maximum transmission at free end point was 13.38. The damping transmission of middle point achieved its peak value at 63 Hz. The maximum transmission at middle point was 3.63.

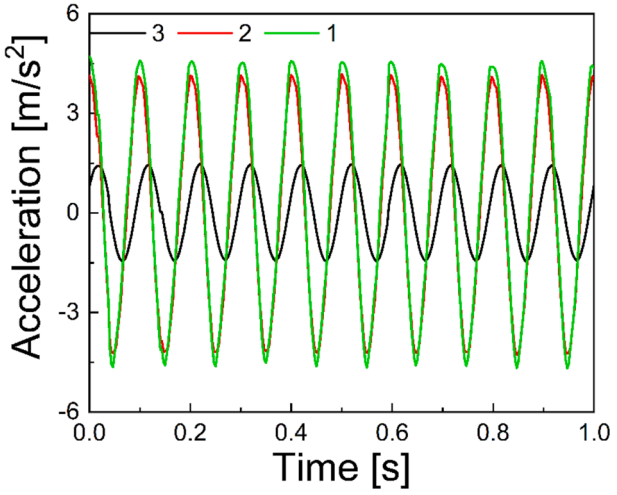

Fig. 7. The vibration mode of 180° sample. The green curve, red curve and black curve illustrated the motion of free end point, the middle point and the fixed point of the cantilever beam. (For interpretation of the references to colour in this figure legend, the reader is referred to the web version of this article.)

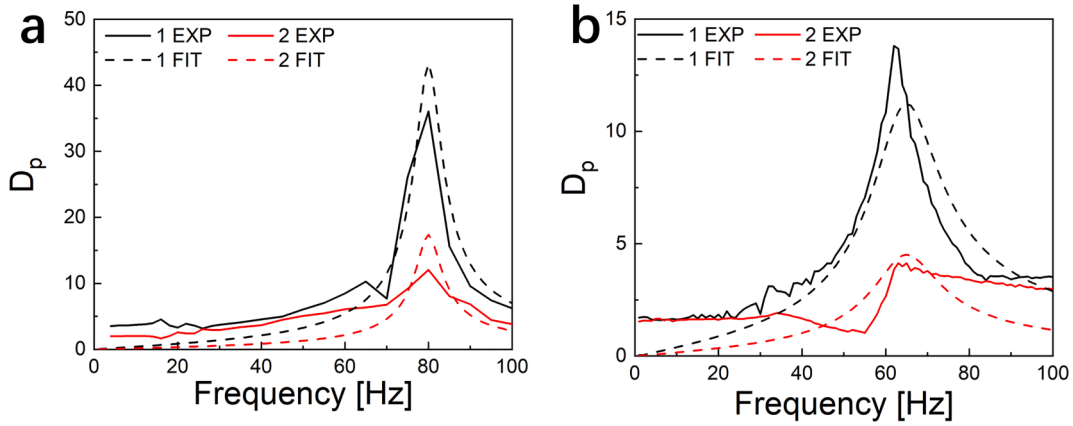

Fig. 8. The vibration mode of 180° sutural beam with core material of (a) PDMS and (b) SSG.

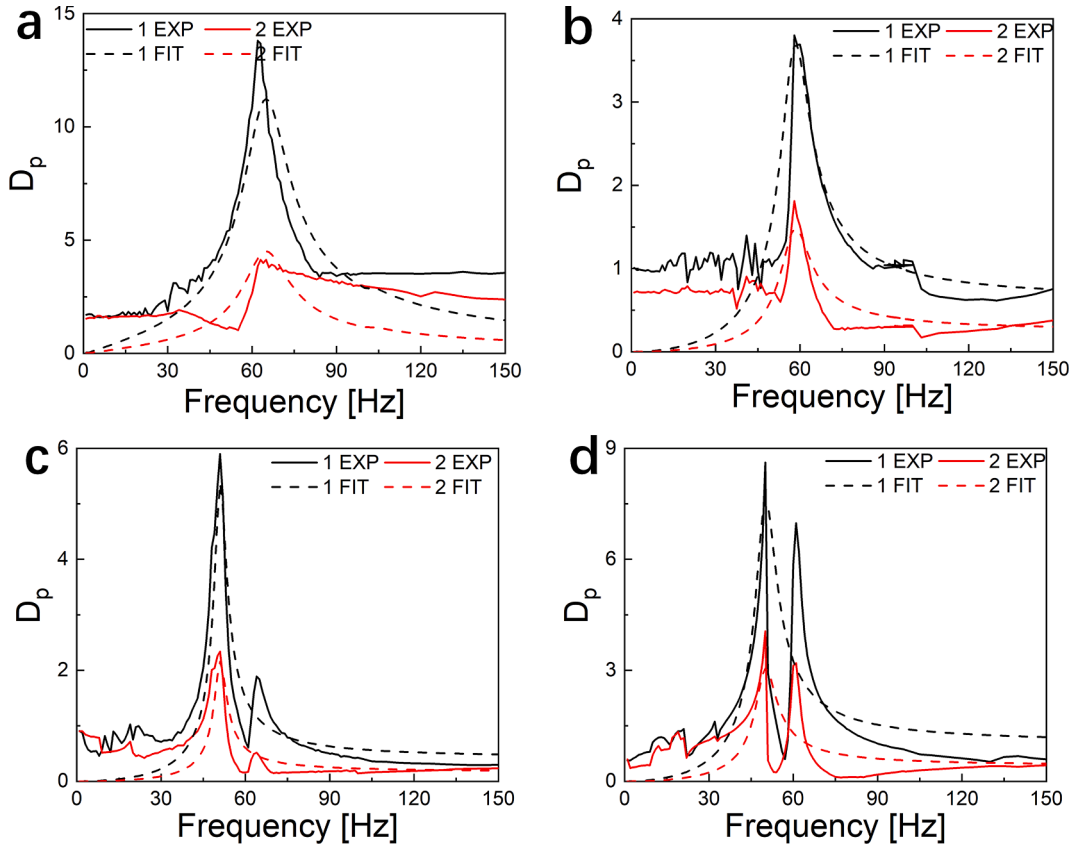

Fig. 9. The vibration mode of different sutural beam composites with SSG core. (a) 180°, (b) 60°, (c) 45°, and (d) 30°. The black lines illustrated the motion of free end point and the red lines illustrated the motion of middle point. Solid curves illustrated the experimental data and the dash curves illustrated the fitting results. (For interpretation of the references to colour in this figure legend, the reader is referred to the web version of this article.)

The suppression of sutural interface on vibration was significant. The peak damping transmission of 60° sutural beam was only 3.80. Compared to the 180° sutural composite beam, the reduction reached 71%. Meanwhile, 45° and 30° sutural composite beams also showed remarkable suppression on vibration. The reductions were 25% and 43%, respectively. The damping transmission of middle point of 180° was 4.13. With the presence of sutural interface, the damping transmission decreased into 1.81, 2.33 and 4.04 with sutural angles were 60°, 45°, and 30°, respectively.

However, the presence of sutural interface geometry led to nonlinear vibration behaviors in the damping transmission. In the classical viscoelastic vibration system, after the first resonance point, the damping transmission would gradually decrease until the next resonance point. However, sutural interface geometry expedited this progress. The nonlinear dynamic response was not obvious in the 180° sutural beam. The damping transmission of 60° sutural beam held 1.04 after 88 Hz and came into a plateau stage. The damping transmission fell to 0.75 when the excitation increased from 91 Hz to 100 Hz. The plateau stage at middle point lasted from 71 Hz to 100 Hz. With the decrease of sutural angles, the nonlinear behavior was further amplified. Under the influence of 45° sutural interface, the cantilever beam achieved its second resonance point at 61 Hz after the first resonance point at 51 Hz. The damping transmission achieved its second peak value of 1.88. The nonlinear vibration behaviors in 30° sutural composite were more

obvious. The damping transmission at the 62 Hz achieved 7.20, which was close to the amplitude at the first resonance. The nonlinear vibration in damping transmission should be owed to the rate-dependent behaviors of SSG core. The elastic modulus of SSG increased with the external excitation frequency, which led to the improvement of structural stiffness of sutural beam. According to the equation (8), the natural frequency should be increased with the external excitation. Sutural interface amplified the local strain. The first resonance point was moved together with the excitation frequency. Then, the second small resonance point was observed.

Considering the rate-dependent of SSG core, the damping behaviors of sutural beams under harmonic excitation with different amplitudes were investigated. The resonance frequency and damping ratio were calculated based on the equation (14). Fig. 10a, b illustrated the damping transmission of the free end point and middle point of 180° sutural beam. 180° sutural beam showed similar vibration behaviors under different amplitudes. However, significant changes could be observed in resonance points and damping transmission. As the amplitude of the source vibration increased from 0.1 mm to 1.2 mm, the resonance point of 180° sutural beam increased from 63 Hz to 86 Hz, and the damping transmission at free end point also gradually increased from 13.38 to 18.01. The vibration in the middle point showed similar behavior. Sutural structure showed more effective vibration isolation behavior under small amplitude vibration. Further, the resonance frequency and damping ratio of different sutural beam under harmonic excitation with different amplitudes were also calculated and shown in Fig. 5.8c, d. With the increase of excitation amplitude, the strain rate of the structure in deformation also increases. The rate-dependent behavior of SSG led to the increase of overall stiffness of the sutural beams, which led to the increase of the resonance frequency. Due to the existence of suture interface, the sutural structure shows higher structural stiffness and higher damping ratio. With the increase of source amplitude from 0.1 mm to 1.2 mm, the resonance frequency of 30° suture structure increases from 70 Hz to 89 Hz, which was similar to that of 45° suture structure. The resonance frequency of changed from 67 Hz to 86 Hz. It showed that there was the highest damping ration in 60° sutural structure, which reached 18.46% when the excitation amplitude was 0.1 mm. The storage modulus of SSG core increased with the increase of excitation amplitudes, which led to the decrease of damping ratio of the whole structures. The damping ratio of 60° sutural beam came to be 11.25% with the amplitude of 1.2 mm. Similarly, the damping ratios of 45° and 30° sutural beams decreased from 14.09% and 12.03% to 8.42% and 8.81%, respectively. The sutural structure showed the advantage of isolating small vibration.

Based on the magnetic-dependent behavior of SSG core, the vibration characteristics of cantilever beam under magnetic field were further studied(Fig. 11). Uniform magnetic fields of 0.1 T, 0.2 T and 0.3 T could be obtained by adjusting the distance between permanent magnets. The experimental results showed that the spatial magnetic field had a significant suppression effect on the structural vibration. The damping transmission factor at the free end point of the 180° sutural beam was rapidly reduced from 13.38 to 7.29. The damping ratio also increased significantly from 11.99 to 15.25. The effect of magnetic field improved the stiffness of SSG in the central layer, which led to the enhancement of the structural stiffness. The resonance frequency was increased from 63 Hz to 68 Hz. At the same time, the magnetic field also provided an additional magnetic damping for the whole structure. Sutural beam was subjected to a magnetic force pointing to equilibrium point, which further improved the suppression of structural vibration.

To conclude, due to the passive and active vibration attenuation performance, this novel sutural composite showed considerable potential in various engineering applications. Higher bending stiffness could help the structure to undertake more loading and maintain stable mechanical behaviors. The passive and active vibration suppression

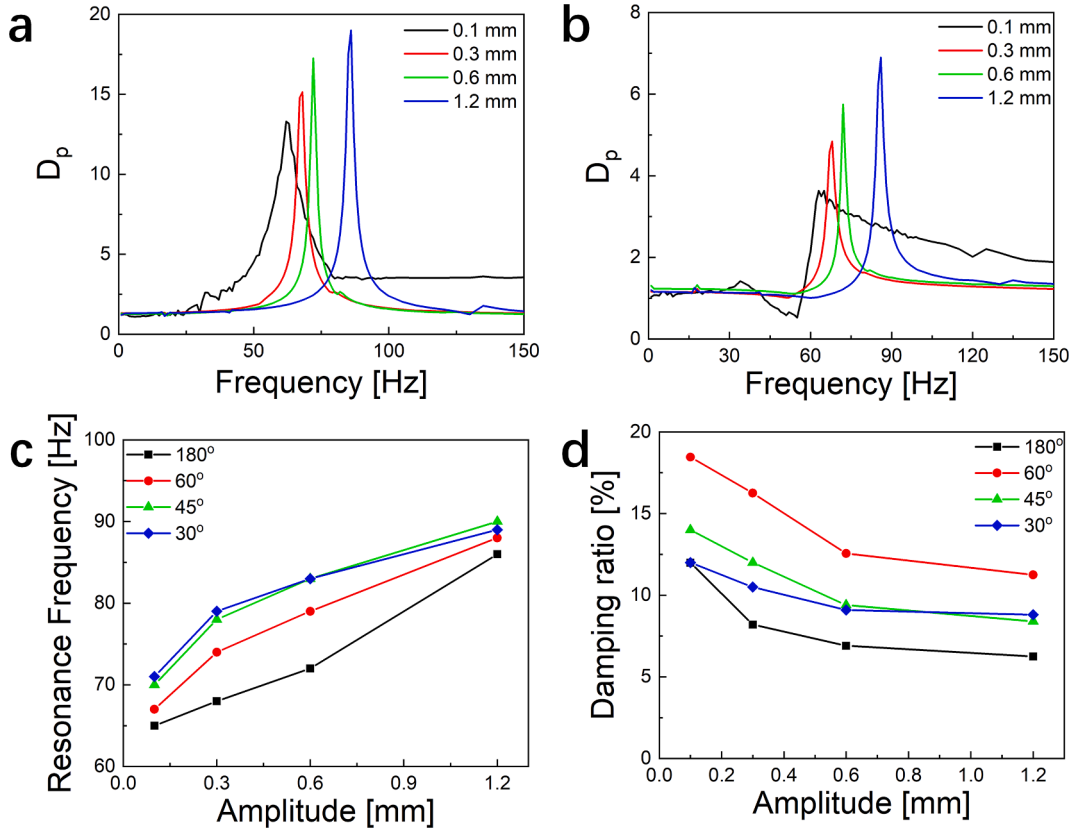

Fig. 10. The vibration mode of free end (a) and middle point (b) of 180° sutural beam under harmonic vibration of different amplitudes. The changes of resonance points (c) and (d) damping ratio of different sutural beam.

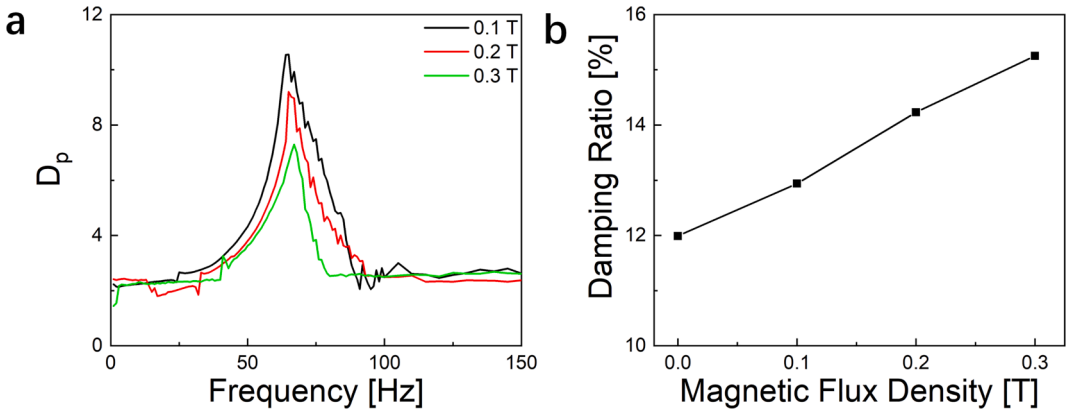

Fig. 11. The vibration mode of free end (a) under different magnetic field and the change of (b) damping ratio of 180° sutural beam.

capacities could be expected to be adopted in some dynamic engineer fields, such as automobile and aircraft suspensions. Meanwhile, it could be used in the milling machine to weaken the vibration during parts processing, and showed potential for turbine blades to suppress the aerodynamic tremor.

4. Conclusion

In this work, four kinds of sutural beam composites with different geometric parameters were prepared with SSG as enhancement material. Three-point bending structure tests with different loading rates were adopted to characterize the effects of sutural interface on the structural stiffness and fracture strength of sandwich beams. The dynamic mechanical behavior was characterized by the vibration test of cantilever beam under stable harmonic excitation with different frequency. Based on the results, the following conclusions could be drawn:

(1) The existence of suture interface could significantly affect the mechanical properties of the structure. Though a certain suture angle reduced the structural stiffness, appropriate angles could effectively improve it. Meanwhile, sutural interface contributed to achieve strain hardening under large deformation, which could improve the failure and softening behavior. Thus, proper angles could expand the fracture deformation limit. To this end, ingenious interface design helped to achieve high structural stiffness or failure strain, so as to adapt to various application requirements.

(2) Compared with PDMS pure elastic material, sandwich beam with SSG core structure held better vibration suppression ability. SSG could effectively reduce the resonance frequency of the beam and obtain attenuated transmission. Owing to the rate-dependent effect, the storage modulus increased as the vibration amplitude raised, resulting in the reduced damping ratio. Thus, the sutural structure showed more effective vibration attenuation performance under small amplitude vibration load. Besides, based on the magneto-rheological behavior, magnetic field could provide an additional magnetic damping for the whole structure, enhancing the suppression capacity for vibration excitations.

(3) The sutural interface could significantly reduce the vibration amplification factor of the cantilever beam. The existence of sutural interface contributed to higher structural stiffness and damping ratio. Meanwhile, it could result in nonlinear vibration behaviors in the damping transmission and amplified the local strain. The proper design of sutural angle could suppress the damping transmission of free end and middle points. In conclusion, this unique sandwich beam structure with sutural interface and SSG core showed a larger damping ratio under small amplitude vibration excitation, which was conducive to isolating small vibration and its engineering application.

CRediT authorship contribution statement

Xiwen Fan: Investigation, Methodology, Formal analysis, Visualization, Writing – original draft. **Yu Wang:** Resources, Methodology, Writing – review & editing. **Sheng Wang:** Methodology. **Xinglong Gong:** Writing – review & editing.

Declaration of Competing Interest

The authors declare that they have no known competing financial interests or personal relationships that could have appeared to influence the work reported in this paper.

Acknowledgments

The authors acknowledge financial supports from the National Natural Science Foundation of China (Grant No. 11972032, 11972337, 12132016, 11772320).

References

[1] Liu Z, Zhang Y, Zhang M, Tan G, Zhu Y, Zhang Z, et al. Adaptive structural reorientation: Developing extraordinary mechanical properties by constrained flexibility in natural materials. Acta Biomater 2019;86:96–108.
[2] Jia Z, Wang L. 3D printing of biomimetic composites with improved fracture toughness. Acta Mater 2019;173:61–73.
[3] Gao C, Hasseldine BPJ, Li L, Weaver JC, Li Y. Amplifying Strength, Toughness, and Auxeticity via Wavy Sutural Tessellation in Plant Seedcoats. Adv Mater 2018;30 (36):1800579. https://doi.org/10.1002/adma.v30.3610.1002/adma.201800579.
[4] Raut MS, Gopalakrishnan S. Elastic and viscoelastic flexural wave motion in woodpecker-beak-inspired structures. Bioinspiration. Biomimetics 2021;16(4): 046021. https://doi.org/10.1088/1748-3190/abf745.
[5] Gupta A, Panda S, Reddy RS. Improved damping in sandwich beams through the inclusion of dispersed graphite particles within the viscoelastic core. Compos Struct 2020;247:112424. https://doi.org/10.1016/j.compstruct.2020.112424.
[6] Ko K, Jin S, Lee SE, Hong J-W. Impact resistance of nacre-like composites diversely patterned by 3D printing. Compos Struct 2020;238:111951. https://doi.org/10.1016/j.compstruct.2020.111951.
[7] de Souza Eloy F, Gomes GF, Ancelotti AC, da Cunha SS, Bombard AJF, Junqueira DM. A numerical-experimental dynamic analysis of composite sandwich beam with magnetorheological elastomer honeycomb core. Compos Struct 2019; 209:242–57.
[8] Miroshnichenko K, Liu L, Tsukrov I, Li Y. Mechanical model of suture joints with fibrous connective layer. J Mech Phy Solids 2018;111:490–502.
[9] Huang T-H, Chen C-S, Chang S-W. Microcrack patterns control the mechanical strength in the biocomposites. Mater Des 2018;140:505–15.
[10] Rayneau-Kirkhope D, Mao Y, Rauch C. Bioinspired Hierarchical Designs for Stiff, Strong Interfaces between Materials of Differing Stiffness. Phys Rev Appl 2018;10 (3). https://doi.org/10.1103/PhysRevApplied.10.034016.
[11] Li Y, Ortiz C, Boyce MC. Stiffness and strength of suture joints in nature. Phys Rev E 2011;84(6). https://doi.org/10.1103/PhysRevE.84.062904.

[12] Li Y, Ortiz C, Boyce MC. Bioinspired, mechanical, deterministic fractal model for hierarchical suture joints. Phys Rev E 2012;85(3). https://doi.org/10.1103/PhysRevE.85.031901.
[13] Al-Furjan MSH, hatami A, Habibi M, Shan L, Tounsi A. On the vibrations of the imperfect sandwich higher-order disk with a lactic core using generalize differential quadrature method. Compos Struct 2021;257:113150. https://doi.org/10.1016/j.compstruct.2020.113150.
[14] Bendenia N, Zidour M, Bousahla AA, et al. Deflections, stresses and free vibration studies of FG-CNT reinforced sandwich plates resting on Pasternak elastic foundation. Comput Concrete 2020;26(3):213–26.
[15] Al-Furjan MSH, Habibi M, Sadeghi S, et al. A computational framework for propagated waves in a sandwich doubly curved nanocomposite panel. Eng Comput-Germany 2020:1–18.
[16] Tahir SI, Chikh A, Tounsi A, Al-Osta MA, Al-Dulaijan SU, Al-Zahrani MM. Wave propagation analysis of a ceramic-metal functionally graded sandwich plate with different porosity distributions in a hygro-thermal environment. Compos Struct 2021;269:114030. https://doi.org/10.1016/j.compstruct.2021.114030.
[17] Zaitoun MW, Chikh A, Tounsi A, et al. An efficient computational model for vibration [17] behavior of a functionally graded sandwich plate in a hygrothermal environment with viscoelastic foundation effects. Eng Comput-Germany 2021:1–15.
[18] Li Y, Ortiz C, Boyce MC. A generalized mechanical model for suture interfaces of arbitrary geometry. J Mech Phys Solids 2013;61(4):1144–67.
[19] Gao C, Li Y. Mechanical model of bio-inspired composites with sutural tessellation. J Mech Phys Solids 2019;122:190–204.
[20] Yu Z, Liu J, Wei X. Achieving outstanding damping performance through bio-inspired sutural tessellations. J Mech Phys Solids 2020;142:104010. https://doi.org/10.1016/j.jmps.2020.104010.
[21] Jia Z, Yu Y, Hou S, Wang L. Biomimetic architected materials with improved dynamic performance. J Mech Phys Solids 2019;125:178–97.
[22] Katayama I. Strength models of the terrestrial planets and implications for their lithospheric structure and evolution. Prog Earth Planet Sc 2021;8(1). https://doi.org/10.1186/s40645-020-00388-2.
[23] Mao L-B, Gao H-L, Yao H-B, Liu L, Cölfen H, Liu G, et al. Synthetic nacre by predesigned matrix-directed mineralization. Science 2016;354(6308):107–10.
[24] Häsä R, Pinho ST. Failure mechanisms of biological crossed-lamellar microstructures applied to synthetic high-performance fibre-reinforced composites. J Mech Phys Solids 2019;125:53–73.
[25] Wang S, Xuan S, Jiang W, Jiang W, Yan L, Mao Ya, et al. Rate-dependent and self-healing conductive shear stiffening nanocomposite: a novel safe-guarding material with force sensitivity. J Mater Chem A 2015;3(39):19790–9.
[26] Wang Y, Ding Li, Zhao C, Wang S, Xuan S, Jiang H, et al. A novel magnetorheological shear-stiffening elastomer with self-healing ability. Compos Sci Technol 2018;168:303–11.
[27] Bajkowski JM, Dyniewicz B, Gębik-Wrona M, Bajkowski J, Bajer CI. Reduction of the vibration amplitudes of a harmonically excited sandwich beam with controllable core. Mech Syst Signal Pr 2019;129:54–69.
[28] Lee N, Williams LN, Mun S, Rhee H, Prabhu R, Bhattarai KR, et al. Stress wave mitigation at suture interfaces. Biomed Phys Eng Express 2017;3(3):035025. https://doi.org/10.1088/2057-1976/aa777e.